Diurnal march of the convection observed during TRMM-WETAMC/LBA

Luiz A. T. Machado, Henri Laurent,[1] and Alexandra A. Lima

Divisão de Ciências Atmosféricas, Instituto de Aeronáutica e Espaço, Centro Técnico Aeroespacial, São José dos Campos, SP, Brazil

Received 8 January 2001; revised 16 July 2001; accepted 11 September 2001; published 6 September 2002.

[1] Radiosonde, satellite data, Tropical Ocean–Global Atmosphere (TOGA) radar 2 km constant altitude plan position indicator (CAPPI), and rainfall collected from the TRMM-Wet Season Atmospheric Mesoscale Campaign (WETAMC)/Large-Scale Biosphere-Atmosphere (LBA) Experiment in Amazonia have been used to investigate the diurnal cycle of the tropical convection. Geostationary Operational Environmental Satellite (GOES 8) images were used to describe the diurnal modulation of the total/high/convective cloud fraction and the diurnal evolution of the size spectrum and initiation/dissipation of the convective systems. Radar 2 km CAPPI were used to describe the diurnal cycle of the rain fraction for different thresholds and the diurnal evolution of the size spectrum and initiation/dissipation of the rain cells. An average over the four rain gauge networks was applied to describe the average hourly rainfall. The upper air network data set was used to compute the thermodynamic variables: equivalent potential temperature (θ_e), convective available potential energy (CAPE), thickness of positive buoyancy, instability, and convective inhibition. High and convective cloud area fractions reach their maximum some hours after the maximum rainfall detected by rain gauge and radar 2 km CAPPI. The minimum cloud cover occurs only a few hours before the maximum precipitation and the maximum cloud cover occurs during the night. The maximum rainfall takes place at the time of the maximum initiation of the convective systems observed by satellite and rain cells. At the time of maximum precipitation the majority of the convective systems and rain cells are small sized and present the maximum increasing area fraction rate. The diurnal evolution of θ_e also presents a very clear diurnal variation, with maximum occurring in the early afternoon. The CAPE is well related to θ_e. When θ_e is high CAPE is high; the atmosphere is unstable and has a deep layer of positive buoyancy and small convective inhibition. These results suggest the following mechanism controlling the diurnal of convection: In the morning, cloud cover decreases as the solar flux reaching the surface increases and consequently increases θ_e. In the early afternoon, convection rapidly develops, high and convective cloud fractions increase rapidly, and the maximum precipitation and initiation is observed. After convection is developed the atmosphere profile is modified, reaching a nearly saturated state; the water vapor flux decreases in the boundary layer which becomes very stable, thereby inhibiting surface fluxes and consequently extinguishing the convection. *INDEX TERMS:* 3314 Meteorology and Atmospheric Dynamics: Convective processes; 3329 Meteorology and Atmospheric Dynamics: Mesoscale meteorology; 3360 Meteorology and Atmospheric Dynamics: Remote sensing; 3374 Meteorology and Atmospheric Dynamics: Tropical meteorology; *KEYWORDS:* convection, cloud cover, diurnal cycle, convective systems

Citation: Machado, L. A. T., H. Laurent, and A. A. Lima, Diurnal march of the convection observed during TRMM-WETAMC/LBA, *J. Geophys. Res.*, *107*(D20), 8064, doi:10.1029/2001JD000338, 2002.

1. Introduction

[2] One of the main characteristics of tropical convection is its strong reaction to diurnal forcing [e.g., *Minnis and Harrison*, 1984; *Duvel and Kandel*, 1985] among others). Knowledge of the diurnal modulation of convection is very useful to verify the diurnal cycle described by general circulation models. Furthermore, this modulation has an important influence on the radiative forcing of cloud cover,

[1]Institut de Recherche pour le Developpement (IRD), France, Cooperation Conselho Nacional de Desenvolvimento Cientifico e Tecnólogico (CNPq), Grenoble, Brazil/IRD.

0148-0227/02/2001JD000338

and thus constitutes a relevant factor for the Earth radiation balance.

[3] The first field campaign of the Large-Scale Biosphere-Atmosphere (LBA) Experiment in Amazonia was held in the Brazilian state of Rondônia in January–February 1999. The campaign known as the Wet Season Atmospheric Mesoscale Campaign (WETAMC/LBA) and the LBA-TRMM was focused on the dynamical, microphysical, electrical, and diabatic heating characteristics of tropical convection in the Amazon region (for a detailed description, see *Silva Dias et al.* [2002]).

[4] The TRMM-WETAMC/LBA experiment combining different measurements allows to describe the diurnal cycle of the clouds, precipitation, and thermodynamics variables. The understanding of the relationships among these parameters and their response to the diurnal cycle is the key question to understand the physical mechanisms and the feedbacks that control the daily variability of the convection.

[5] Infrared radiation in the atmospheric window is very sensitive to both surface temperature and cloud cover, especially deep convective clouds. Many properties of the diurnal cycle of the convection over South America have been described by geostationary satellites data. *Minnis and Harrison* [1984] examined the diurnal cloud variability for one month (November 1978) from hourly Geostationary Operational Environmental Satellite (GOES 8) high-resolution image, documenting regionally the diurnal variations in low, middle, and high cloudiness. *Hendon and Woodberry* [1993] investigated the diurnal cycle from one-year global imagery constructed from infrared channel; they analyzed the brightness temperature and deep convective activity describing the global distribution of amplitude and phase of the diurnal cycle. *Janowiak et al.* [1994] described the diurnal character of cold cloudiness in oceanic tropics during the period 1986–1990 using fractional coverage of cold clouds for three different temperature thresholds. *Guedes and Machado* [1997] using ISCCP (International Satellite Cloud Climatology Project) data described the diurnal variation of the cloud cover over the South America. *Garreaud and Wallace* [1997] studied the diurnal cycle over the Americas using ISCCP data and rainfall estimates based on microwave SSM/I imagery. They concluded that in general way cloudiness over land tends to occur in the late afternoon.

[6] *Silva Dias and Bonatti* [1985] and *Silva Dias et al.* [1987] examined the diurnal variation in the thermodynamic structure and the divergence fields using a numerical weather model over the Amazon region. These studies showed the importance of diurnal variations, especially to relate large-scale fields to the tropical troposphere response to diurnal forcing in the Amazon. Near coastlines the land-sea-breeze circulation can explain much of the diurnal cycle of clouds and precipitation. The diurnal cycle of convective cloudiness, in the North of Brazilian coast and parts of the Central Amazon Basin, is related to the activity of squall lines generated by coastal region sea breeze. *Garstang et al.* [1994] and *Cohen et al.* [1995] pointed out the importance of squall line activity to the total precipitation over the rain forest of the central Amazon basin and its relation to the sea-land-breeze. The Rondônia state is far away from the coast and consequently the action of these squall lines is reduced, solar heating and large-scale features mainly modulate the diurnal cycle.

[7] *Machado* [2000], analyzing data from ABLE-2B and FluAmazon experiments, suggested that the solar flux absorbed by the surface is always smaller than the total surface flux supplied to the atmosphere during convective events and always larger during nonconvective events. This means that the surface loses more energy than it receives during convective events and vice versa. The surface energy never seems to be in equilibrium. However, the quantity of energy stored at the surface seems to be limited, defining a timescale, that determines when surface and atmosphere need to export or receive energy in order to balance their deficit or excess of energy. The process that controls this deficit/excess of energy within the diurnal timescale will be discussed here based on the thermodynamic variables and the different characteristics of the cloud cover variability.

[8] The main goal of this study is to describe the diurnal cycle of the different cloud types, of the rain observed by the radar (reflectivity) and of the thermodynamics variables. The relationships between those parameters would allow understanding the physical mechanisms that control the cloud cover variability.

[9] In section 2 we present the data and methodology used. Section 3 presents the diurnal cycle of the cloud cover and radar reflectivities. Section 4 deals with the structural and morphological characteristics of the diurnal organization of the convective cloud cover. In section 5 we discuss the behavior of the thermodynamic parameters and their diurnal variation. Section 6 summarizes the results.

2. Data and Methodology

[10] This study uses four sources of data: GOES 8 infrared brightness temperature images, the 2 km constant altitude plan position indicator (CAPPI) from NASA-C Band Doppler weather radar, known as Tropical Ocean–Global Atmosphere (TOGA) radar, precipitation measurements from a rain gauge network and radiosondes released at Rebio Jarú, Rolim de Moura, and Abracos during the TRMM-WETAMC/LBA experiment.

[11] GOES 8 images were preprocessed by NASA-GSFC. The raw data were converted to brightness temperature and later to count and stored in 8 bit TIFF images. Navigation files were created periodically during the experiment period. The horizontal resolution is 4 km × 4 km at the nadir. During the LBA experiment the images were available every half hour, according to NOAA-GOES scanning strategy. Continuous series of cloud fraction were built using these images, for different brightness temperature thresholds, over a 2.3° × 2.3° area covering the WETAMC/LBA region (longitude: −63.3° and −61.0° and latitude: −12.1° and −9.8°). Cloud Fraction was computed for the following infrared GOES channel 4: brightness temperature (Tir) thresholds: Tir < 284 K, Tir < 273 K, Tir < 265 K, Tir < 245 K, Tir, 235 K, Tir < 225 K, Tir < 210 K, and Tir < 200 K. These thresholds were chosen based in the general histogram of the Tir over the TRMM-WETAMC region (Figure 1a). These thresholds intend to describe a measure ranging from the total cloud cover (warmer thresholds) to the convective cloud cover (colder thresholds).

[12] Figure 1 shows the histogram of the Tir for different hours. The thresholds used in this study are also indicated in the figure. We can see two different patterns: One is mainly

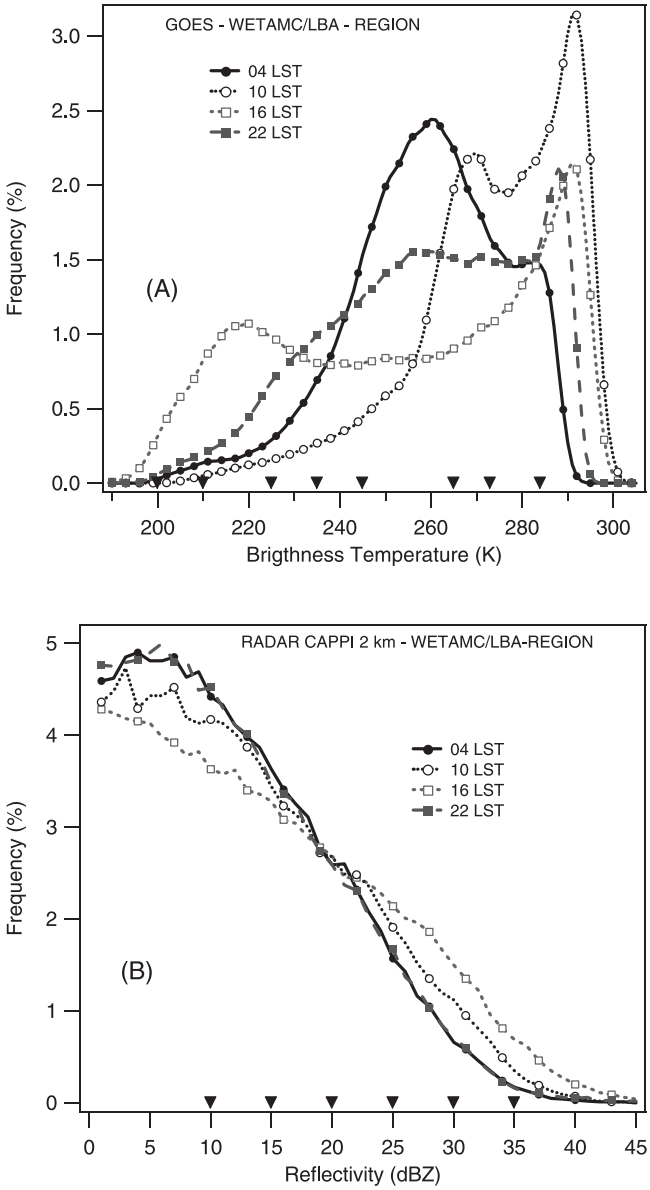

Figure 1. Histogram of the brightness temperature (a) from GOES 8 images and the reflectivity from 2 km CAPPI TOGA radar (b). The histogram was computed for the TRMM WETAMC/LBA region (longitude: −63.3° and −61.0° and latitude: −12.2° and −9.8°) for the period from 9 January to 27 February 1999. The histograms are presented for 0400, 1000, 1600, and 2200 LST.

associated with clear sky emission (Tir warmer than about 284 K) and another with cloud emission (Tir colder than about 284 K). The limit between the clear sky distribution and the cloud distribution is not obvious. The atmospheric mixed layer temperature, during the experiment, was always larger than 287 K. Due to the large amount of water vapor close to the surface the absorption of infrared radiance by this gas was strong, thus clear sky brightness temperature measured by the satellite is more associated to the mixed layer brightness temperature than to the surface brightness temperature. Thus, the threshold of 284 K, slightly colder than the atmospheric mixed layer temperature, was the one chosen to estimate the total cloud cover. We also used the thresholds of 273 K and 265 K to have a detailed description of the cloud cover.

[13] The coldest part of the histogram, below 245 K, is likely to be associated with convective cloud cover, including thick Cirrus, high levels thick stratiform clouds and Cumulus Nimbus. *Rickenbach* [1999] and *Wu and LeMone* [1999] studied the cloud top evolution of tropical squall lines during TOGA-COARE. They found that the coldest clouds were more closely associated with weaker surface precipitation because cold cloud shield became spatially decoupled from the source convection. They concluded that cold brightness temperature cloudiness implies that deep convection is or recently was active. Cold brightness temperature threshold is more related to the convective part of the cloud cover in the time/space-averaged sense than for instantaneous images. The size distribution of the coldest part of the convective systems obtained from instantaneous image should not be interpreted as the precipitation portions but as the higher and deeper portions of the convective system. *Machado and Rossow* [1993] discussed the thresholds suitable to describe the convective clouds over the whole globe. They concluded that, in general, image pixels containing high level clouds are identified by brightness temperature smaller than 245 K and convective parts by brightness temperature smaller than 215 K. *Maddox* [1980], *Miller and Fritsch* [1991], and *Machado et al.* [1998] identified mesoscale convective systems as clouds with thresholds of Tir between 241 K and 245 K, and the most active convective parts, embedded inside the convective systems, by thresholds of Tir between 221 K and 215 K. In this study we have used 4 thresholds to identify the different convective parts of the total cloud cover by the thresholds 245 K, 235 K, 225 K, 210 K, and 200 K. Continuous hourly series of the different cloud fractions were constructed by averaging the cloud fractions observed each hour as representative of the observation of the middle of the hour. These series were used to determine the average hourly variation of the cloud fraction.

[14] The TOGA radar has a wavelength of 5.4 cm, a beam width of 1.65 degrees and a peak power of 250 kW. It is operated with a pulse width of 2.0 μs and gate width of 250 m covering a region of 150 km radius. Complete volume scans were performed every 10 minute intervals (sometimes more frequently) accomplishing elevations from 0.5 up to 30.0 degrees or higher. In this study we have used the 2 km CAPPI based on weight beam volumes. The weight and the 3-D position are precomputed based on the elevation/range of the radar. The horizontal resolution of the CAPPI was set to 5 km × 5 km in order to have nearly the same spatial resolution of GOES images.

[15] Figure 1b presents the histogram of the reflectivity (REF) of the CAPPI over the same region used for satellite cloud fraction. Reflectivity fraction was calculated for different thresholds (REF > 10, REF > 15, REF > 20, REF > 25, REF > 30, and REF > 35 dBZ). Thresholds bellow 10 dBZ were not considered due to very small signal/noise relationship. We can note that the reflectivity distribution fits a section of Gaussian function. The distribution is very smoothed and the selection of the six thresholds was defined linearly (5 dBZ interval) up to 35 dBZ. The upper limit of 35 dBZ is a little smaller than some authors have used to describe convection but it was defined to have a

significant statistical population of pixels, the average diurnal peak of the 35 dBZ area fraction is not larger than 1.5%, the histogram in Figure 1b shows the population of values larger than 35 dBZ. The reflectivity fraction intends to describe the rain distribution at 2 km height for different rain intensities. It will be called *rain fraction* hereafter. A continuous hourly series was constructed averaging the rain fraction inside one hour as representative of this hour.

[16] Cloud fraction and rain fraction were computed from 9 January to 27 February as:

$$F_S = \frac{100}{N}\sum_{i=1}^{N}\partial_i \rightarrow \left\{\begin{array}{l}\partial_i = 1, Tir < Threshold\\ \partial_i = 0, Tir \geq Threshold\end{array}\right\}$$
$$F_R = \frac{100}{N}\sum_{i=1}^{N}\partial_i \rightarrow \left\{\begin{array}{l}\partial_i = 1, REF > Threshold\\ \partial_i = 0, REF \leq Threshold\end{array}\right\} \quad (1)$$

where F_s and F_r are the cloud fraction and the rain fraction from satellite radiances and from CAPPI 2 km TOGA radar reflectivity respectively.

[17] The rain gauge network was distributed in four clusters. The rain gauge tipping buckets have a sampling resolution of 0.254 mm and maximum temporal resolution of 10 s. We used in this study the hourly cumulated rain gauge data from the Goddard DAAC (Distributed Active Archive Center). An average over the 4 networks was applied to describe the average hourly rainfall over the TRMM-WETAMC region.

[18] To compute the thermodynamic parameters we have used the upper air network data set operating during the WETAMC/LBA. The radiosondes were released every three hours at (0000 UTC to 2100 UTC) and data collection was conducted from 9 January (only Abracos) to 28 February. The simultaneous radiosonde releases, for the three sites, cover only the period from 24 January to 20 February. The data used in this study has passed a preliminary quality control. The data vertical resolution employed in this work is 40 hPa. Due to the strong influence of the surface observation in the computation of the thermodynamic parameters and some uncertainties in surface observation data we have computed the thermodynamic variable first level using an average of the first 40-hPa layer. Differences between Vaisalla and VIZ system and uncertainties in the radiosonde measures in TRMM-WETAMC/LBA are discussed by G. Fisch et al. (The convective boundary layer over pasture and forest in Amazonia, submitted to *Journal of Geophysical Research*, 2001, hereinafter referred to as Fisch et al., submitted manuscript, 2001).

3. The Diurnal Cycle of Cloud and Rain Fraction

[19] The average hourly cloud fraction was computed, for the different thresholds, in order to present the typical diurnal variation of the different cloud types. Figure 2a shows the hourly average cloud fraction for the thresholds 284 K (close to total cloud cover), 235 K (high cloud cover), and 210 K (clouds associated with the deep convection as seens by satellite). Three different scales are presented in this figure, because of the large variations among the different cloud fraction. Indeed, the total cloud cover varies from 56% to 94%, the high cloud fraction from

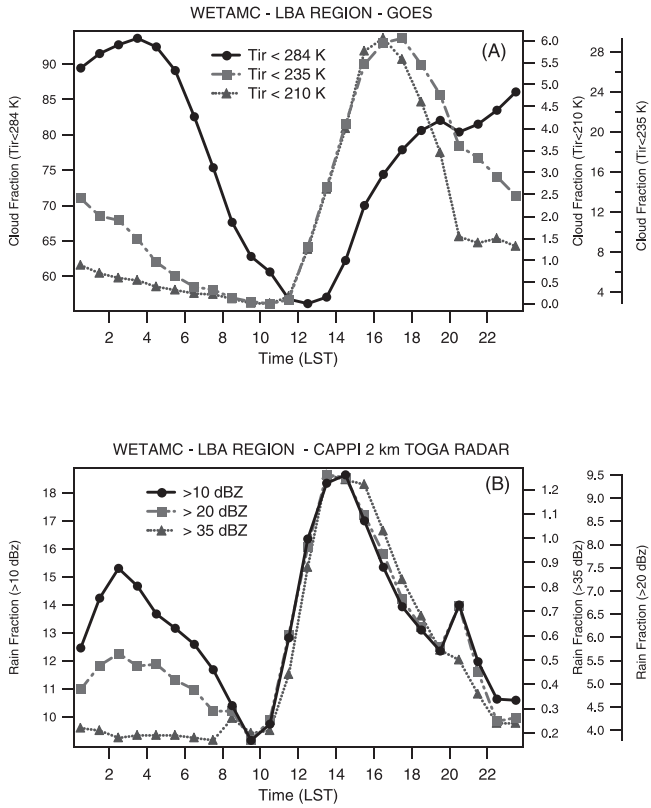

Figure 2. Hourly average cloud fraction (a) for the brightness temperature threshold of 284 K, 235 K, and 210 K, and for rain fraction (b) defined as the fraction larger than 10 dBZ, 20 dBZ, and 35 dBZ, for the period from 9 January to 27 February 1999. Each cloud fraction is presented in a specific scale.

3% to 29% and the deep convective cloud fraction from 0% to 6%.

[20] The 210 K cloud fraction peaks at 1630 LST and the 235 K cloud fraction at 1730 LST, i.e., deep convective cloud fraction peaks one hour earlier than high cloud fraction. A similar short time phase lag from very cold to warmer cloud top was also found in some other studies [e.g., *Chen and Houze*, 1997; *Garreaud and Wallace*, 1997]. We observe for both cloud fraction (convective and high clouds) a strong increase after 1130 LST with a maximum cloud fraction increase rate around 1330 LST. After the maximum, deep convective fraction shows a fast decrease between 1630 and 2030 LST, with a maximum decrease rate at 1930 LST. After 2030 LST we observe a break and the coldest cloud fraction decreases slowly during the night presenting a very small average convective cloud fraction. For high cloud fraction we observe nearly the same behavior, however, it does not decrease as fast as convective cloud fraction. After 2030 LST high cloud fraction shows a slow decrease from 18% to almost 0% at 1130 LST, in the next day morning. For the total cloud fraction [284 K] a completely different behavior is observed. The total cloud fraction peaks at 0330 LST with an average of 94%. During nighttime the total cloud fraction is always larger than 80% on average. *Minnis and Harrison* [1984] studying the diurnal variability of regional cloud distributions show a

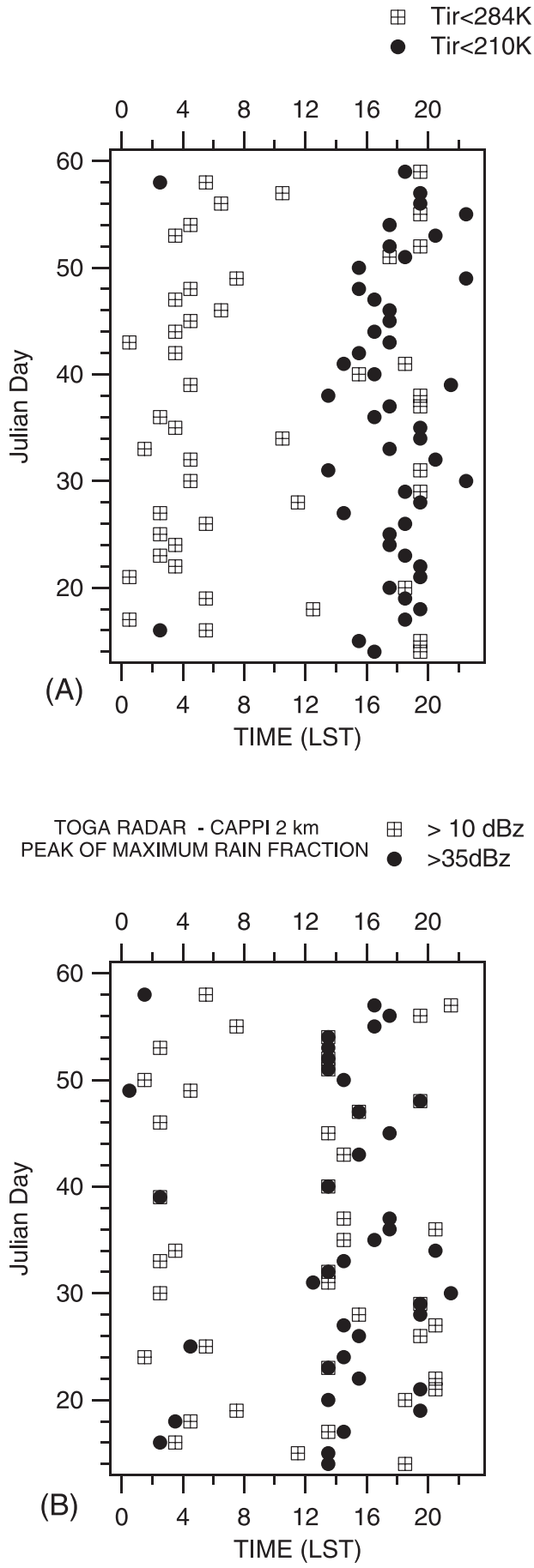

nocturnal maximum in the total cloudiness over Rondônia region. *Duvel* [1989] studying the diurnal variation of low and midlevel cloud over tropical Africa found the same feature, a very strong diurnal modulation with maximum coverage between 0300 LST and 0600 LST. After the maximum, the total cloud fraction decreases slowly up to 1230 LST. Minimum total cloud fraction happens at the time when high and convective cloud fraction have the maximum increase rate; it means that convection starts to develop when the total cloud cover is minimum and solar flux is around the maximum, at the time when the maximum solar radiation reaches the surface. The total cloud fraction, that accounts for a much larger amount of cloud cover than the high and convective fraction (around 3.5 times the high cloud fraction and 12.0 times the convective cloud fraction) has a secondary peak at 1930 LST when high and convective clouds have the maximum decreasing rate. This result suggests that high clouds might evolve to middle and low-level clouds and/or become thinner, with a smaller emissivity. One hour after the secondary maximum, around 2030 LST, the total cloud fraction increases again to reach the night maximum at 0330 LST as mentioned before. The nighttime cloud cover has an important impact in the energy radiation budget by reducing the outgoing longwave radiation and increasing the energy stored in the subcloud layer.

[21] The histogram in Figure 1a clearly presents the diurnal evolution of the different cloud covers. We can see at 1600 LST a large number of pixels around 220 K followed by an increased population of pixels between 240 K to 260 K at 2200 LST. At 0400 LST this large population of pixels moved around 260 K and around 270 K at 1000 LST. These behaviors reveal the change in the cloud cover during the day from deep convective clouds at 1600 LST to middle and low clouds during the night and early morning. Due to the semitransparent clouds (mainly thin Cirrus clouds) that bias the cloud cover classification, at 2200 LST the large population of pixels between 240 K and 260 K is, probably related to a mixing of clouds with different emissivities and cloud tops. The relative humidity profiles presented later in Figure 5 will clarify the diurnal evolution of the cloud types.

[22] Some nocturnal mesoscale convective systems crossed the WETAMC/LBA region during the experiment (for a complete discussion about mesoscale convective systems, see *Laurent et al.* 2002). One can question whether the average nighttime maximum in the total cloud cover is a consequence of these sporadic nocturnal squall lines or not. Figure 3a presents the time of maximum cloud fraction, for each day, for the thresholds 284 K and 210 K. For the majority of the days, the total cloud fraction peaks during night (around 0200–0400 LST) and the convective cloud fraction peaks during the afternoon (around 1600–1900 LST). For some days only the total cloud fraction occurs in the afternoon, probably associated with stronger convective activity, but in such cases a secondary peak is also observed during the night. The convective cloud fraction shows an almost systematic maximum in the late afternoon. The maximum convective fraction occurs during the night for

Figure 3. (opposite) Diagram day versus local time showing the moment of the maximum 284 K and 210 K cloud fraction (a) and 10 dBZ and 35-dBZ-rain fraction (b).

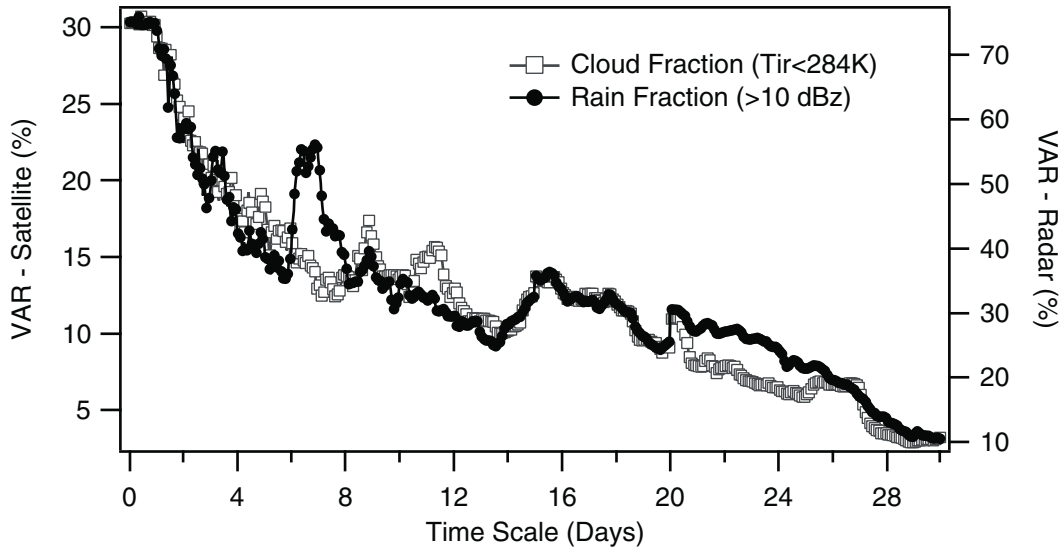

Figure 4. Average difference, expressed in percentages, between hourly distributions obtained from the timescale (days) and the hourly distribution obtained for the whole period. For timescale equal 1, VAR correspond to the difference between each day and the average distribution. The distributions are presented for total cloud fraction (284 K) and rain fraction (10 dBZ).

only a few days. The convective cloud fraction for situations of nocturnal maximum is not larger than the average afternoon convective cloud fraction, thus the results from Figure 3a show that the sporadic nocturnal convection does not bias the average distributions.

[23] The average hourly rain fraction was computed for the different thresholds, in order to present the typical diurnal variation in the rain-reflectivity intensity field. Figure 2b shows the hourly average rain fraction for the thresholds: REF > 10 dBZ (any type of rain - close to the total rain fraction at 2 km height), REF > 20 dBZ (weak to moderate rain at 2 km height) and REF > 35 dBZ (more intense rain at 2 km height). Three different scales are presented due to the amplitude that varies from 18% to 9% for the total rain fraction, from 3% to 10% for the moderate rainfall area fraction and from 0% to 1.5% for the intense rain area fraction.

[24] The three rain fraction peak in the early afternoon, at the same time, around 1330–1530 LST. Differently from the cloud fraction, the total, moderate, and intense rain fractions have their maxima at the same time. They present a rapid increase between 1030 to 1430 LST, at the time of minimum total cloud cover, and a slow decrease from 1430 to 2230 LST. A secondary peak for moderate and light rainfall was noted around 2030 LST, probably associated to the late occurrence of some diurnal convection. During the night a secondary peak is observed associated with light to moderate rainfall in agreement with the results obtained for cloud fraction. The minimum rain fraction occurred, for all thresholds, around 0930 LST. It can be seen in the histogram showed in Figure 1b that the shape of the curves do not change during the diurnal cycle. Nevertheless, the slope of the histograms change during the time evolution where 20 dBZ level remains constant during the entire day.

[25] Figure 3b presents the time of the maximum rain fraction, for each day, for REF > 10 dBZ and REF > 35 dBZ. The hour of maximum occurrence is more variable for the total rain fraction than for the total cloud fraction. Sometimes the daily maximum happens in the afternoon sometimes during the night. However, as it was discussed for the cloud fraction, a maximum total rain fraction in the afternoon does not mean that a secondary maximum was not observed during the night. Although for the majority of the days the maximum intense rain fraction (REF > 35 dBZ) occurred in the afternoon, around 1430 LST, for some days it occurs during the night. Rain fraction has a much larger variability than cloud fraction.

[26] To have an idea about how representative is the average diurnal variation of the cloud cover and of the rain fraction showed in Figure 2, we have computed the variability of these distributions as follows:

$$VAR(k) = \frac{\left\{\frac{1}{M}\sum_{i=1}^{m=N/k}\left\{\frac{1}{24}\sum_{h=1}^{24}\left(f_i^k(h) - F(h)\right)^2\right\}\right\}}{\frac{1}{24}\sum_{i=1}^{24}F(h)} * 100 \quad (2)$$

where, N is the number of days, F(h) is the average hourly cloud or rain fraction obtained for the N days (the whole period), $f_i^k(h)$ is the average hourly cloud or rain fraction over the period of k days (k varies from 1 to N/2) computed in the i^{eme} part of the data set. VAR (k), corresponds to the average difference, expressed in percentage, between the hourly distribution obtained over k days and the hourly distribution obtained for the whole period. For example, VAR(1) corresponds to the difference between each day and the average distribution.

[27] We can see in Figure 4 that for k varying from 1 to 5 days, VAR(k) decreases exponentially from 30% to 13% for the cloud fraction, and from 70% to 35% for the rain fraction. As mentioned before, the rain fraction has a larger variability

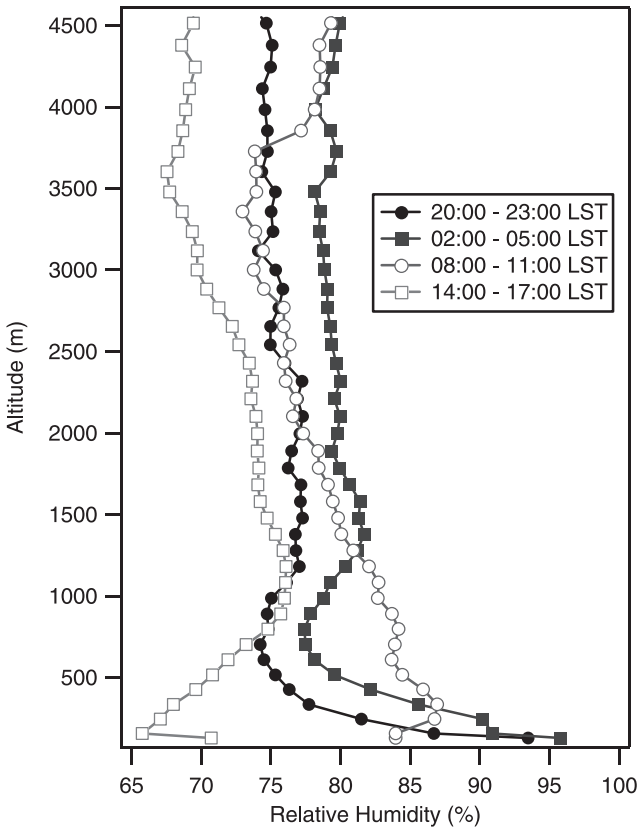

Figure 5. Relative humidity average profile for 2000–2300 LST, 0200–0500 LST, 0800–1100 LST, and 1400–1700 LST for Rebio Jaru station from surface to 4500 m.

than the cloud fraction and the average distribution should be interpreted carefully. Larger rain fraction variability is expected because rain is an internal feature of the total cloud cover, having a shorter time/space scale than the cloud top. For k > 5 days, the error slowly decreases linearly with the timescale. This result shows that the variability of the diurnal cycle of cloud and rain fraction is very high but decreases rapidly up to 5 days; for timescale larger than 5 days this variability decreases slowly and the diurnal cycle is very close to that one described by 30 days average.

[28] To describe the diurnal variation of cloud fraction and rain fraction better, we have computed the hourly averaged relative humidity profiles measured in the Rebio Jaru site. Figure 5 shows large diurnal variation of the relative humidity profile from surface to 4500 m. We notice a very high average relative humidity near the surface during the nighttime, probably related to the shallow nocturnal boundary layer height. From around 1000 m up to 4500 m the average relative humidity profile for 0200–0500 LST presents the largest values around 82%. Its likely to corresponds to low-level clouds that systematically form in this layer in agreement with the total cloud cover fraction observation. High average relative humidity values, at these levels, are probably due to a systematic cloud layer. During the morning (0800–1100 LST), at the same time as the Sun rising and insolation increases, low level clouds beginning to dissipate. Figure 5 shows, at this time, the largest average relative humidity at the layer from around 300 m to 1000 m. The specific humidity profile (not shown) reveals that the atmosphere, in the early afternoon, is dryer in the boundary layer and becomes wetter in the following hours showing the typical behavior of the diurnal convection. *Machado* [2000] described the energy stored in the atmosphere after convection in the Amazon Basin; he showed that a large amount of latent energy is stored in the middle atmosphere as a consequence of the vertical water vapor flux due to the convective towers.

4. The Spatial Organization of Clouds and Reflectivities

[29] *Miller and Fritsch* [1991] and *Machado et al.* [1992] described the structural properties of the tropical cloud clusters, observed from satellites images. They show a nearly equal contribution of all cloud cluster sizes to the mean high cloud cover, when data is integrated over a long period. However, for specific analysis such as different times of the day and different phase of synoptic perturbation, the cloud cluster size distribution can be very useful. *Machado et al.* [1993] describe the typical behavior of the cloud organization for the diurnal cycle over the Atlantic Ocean and West Africa using the cloud cluster size distribution. *Machado and Rossow* [1993] have used the 245 K threshold to describe high level clouds over the whole globe. In the present work we have defined high level clouds as the area covered by adjacent pixels (in GOES image) having Tir smaller than 235 K. This threshold is colder than former used because higher spatial resolution images is being used and the Tir average histogram shows that 235 K is more adapted to describe the high level clouds at this specific region. We computed the location of the center and the area covered by the convective system. Because of the large range of convective system shapes observed, we compute an effective radius (called as radius hereafter), assuming a circular shape. What we call radius is then only a convenient linear measure of the convective system area. In the present study we have taken into account only the convective system whose center crossed the LBA region, as defined in the data section.

[30] The same procedure was applied to the radar data, using the CAPPI 2 km and the threshold of 20 dBZ. The adjacent pixels in the CAPPI image with reflectivity larger than 20 dBZ will be called rain cell. Studies based on ground and aircraft-based meteorological measurements define a convective cell as a region of high speed updraft within cumulonimbus clouds; the size of these cells is less than equal to 20 km [*Cotton and Anthes*, 1989], larger than the typical size of individual satellite pixels. Radars detect only the precipitation sized particles, not the smaller particles composing the clouds. The radar echoes of these systems, defined by radar reflectivities greater than 35 dBZ are commonly defined as convective core or convective cells. The spatial organization of the rain cells corresponds to the organization of moderate to intense rain at 2 km height.

[31] Convective system describes the cloudiness mesoscale organization and the rain cell defines the rain feature as an intimate part of the convective systems, which will be called hereafter as only convective system and rain cell. The distributions of convective systems and rain cells area fraction as function of the radius were computed for each

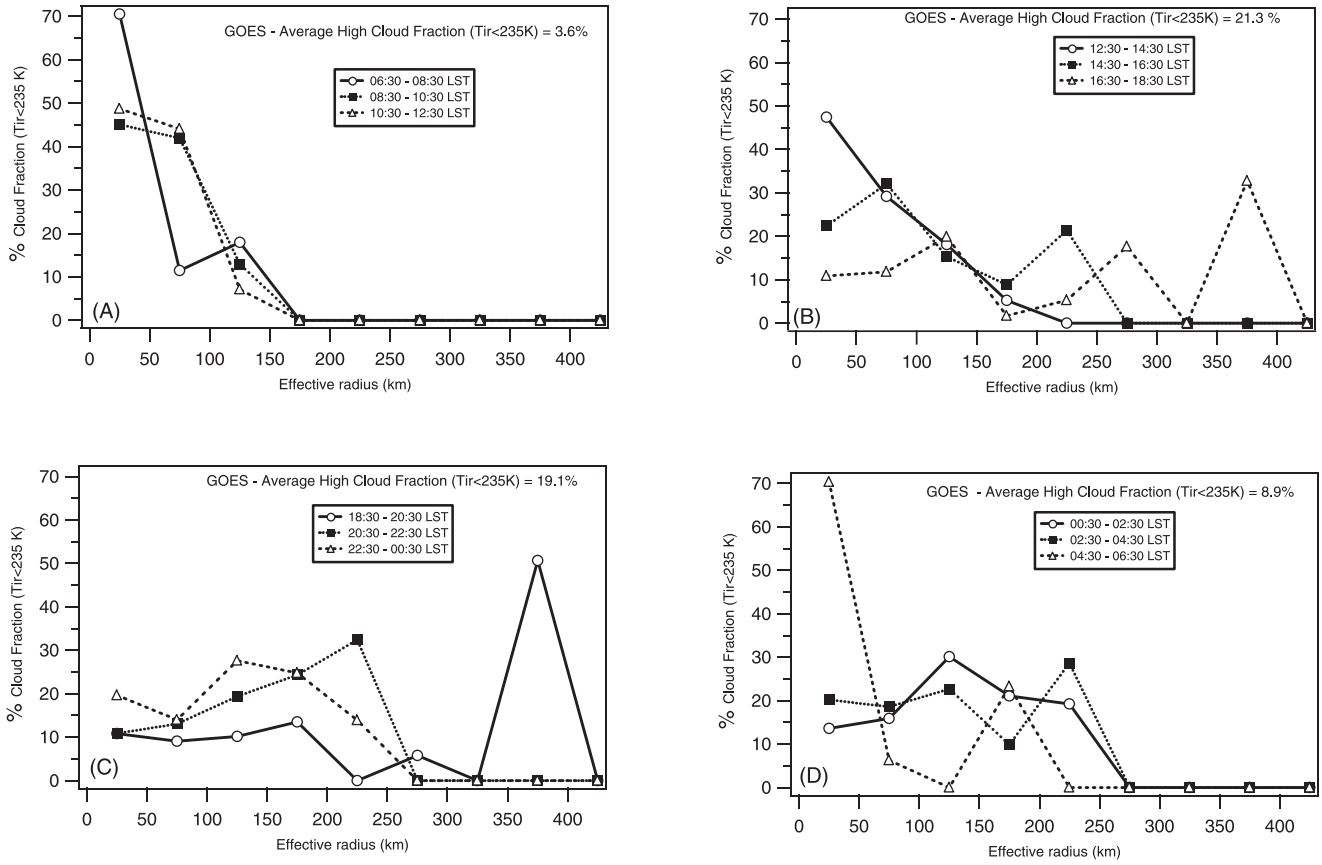

Figure 6. Convective system size distribution as function of the diurnal cycle. Convective system were defined using the threshold of 235 K. Distributions are presented as the two-hours average. The curves show the contribution to the total cloud cover at specific time by different convective system radius size.

two-hour. It describes the relative contribution of high cloud cover (moderate rain fraction) for a given radius class as follows:

$$S(\Delta r) = \frac{1}{s_t} \sum_{r=r1}^{r2} s(r) \qquad (3)$$

where S(Δr) is the contribution to the total high cloud cover (S_t) of the convective systems having a radius in the Δr size interval (from r_1 to r_2); s(r) is the area of the system with radius r. The distributions are normalized by the total fraction (S_t) therefore, do not take into account the diurnal variability of the cloud fraction.

[32] Figure 6 shows the size distributions of the convective system for different hours. This figure presents the spatial scale involved in the diurnal evolution showed in Figure 2. In the early morning the majority of the high cloud cover is organized in small-scale systems, during the period 0630–0830 LST, 70% of the convective systems have a size around 25 km. The size distribution for the period 0830–1230 LST shows that high cloud cover is also dominated by small spatial scale but with a slight increase in convective systems size. In the afternoon between 1230 and 1830 LST we observe a progressive increase in the spectrum of the cloud size. At 1430–1630 LST only 22% of the cloud cover is due to small systems, at this time two spatial scale dominate the spectrum: 75 km and 225 km. Later on, only 10% of the high cloud cover is organized in small scale and convective systems become larger with typical sizes of 250 and 375 km. Around 1830–2030 LST almost the entire high cloud cover is organized into large convective systems. During the evening the spatial scale of the convective systems decreases to around 100 to 200 km. This typical convective system size persists during the whole night. At the end of the night and at dawn the large convective systems are nearly dissipated and the high cloud cover presents a small-scale organization. A general behavior of the spatial scale diurnal variability can be described as an increase in the convective system size organization from the early afternoon to the early night. After convective systems reach the maximum spatial scale organization (an average size of 250 km), they are followed by a fast decrease to a medium size, around 140 km radius, maintaining this spatial scale up to the early morning when high cloud cover becomes organized in very small scale.

[33] Figure 7 presents for different hours the size distribution of the rain cells (REF > 20 dBZ) computed from the TOGA radar 2 km CAPPI. We note that the rain cell size distribution during the whole night and in the morning have approximately the same shape: Around 12% of the total rain fraction is from cells with radius around 5 km (except at some hours we observe a slight maximum for 15 km radius); a constant contribution of around 15% for rain cells size up to 30–40 km, followed by a nearly linear decrease. The most remarkable difference in the size spectrum during this period can be noted at night (0030 to 0630 LST) when a maximum

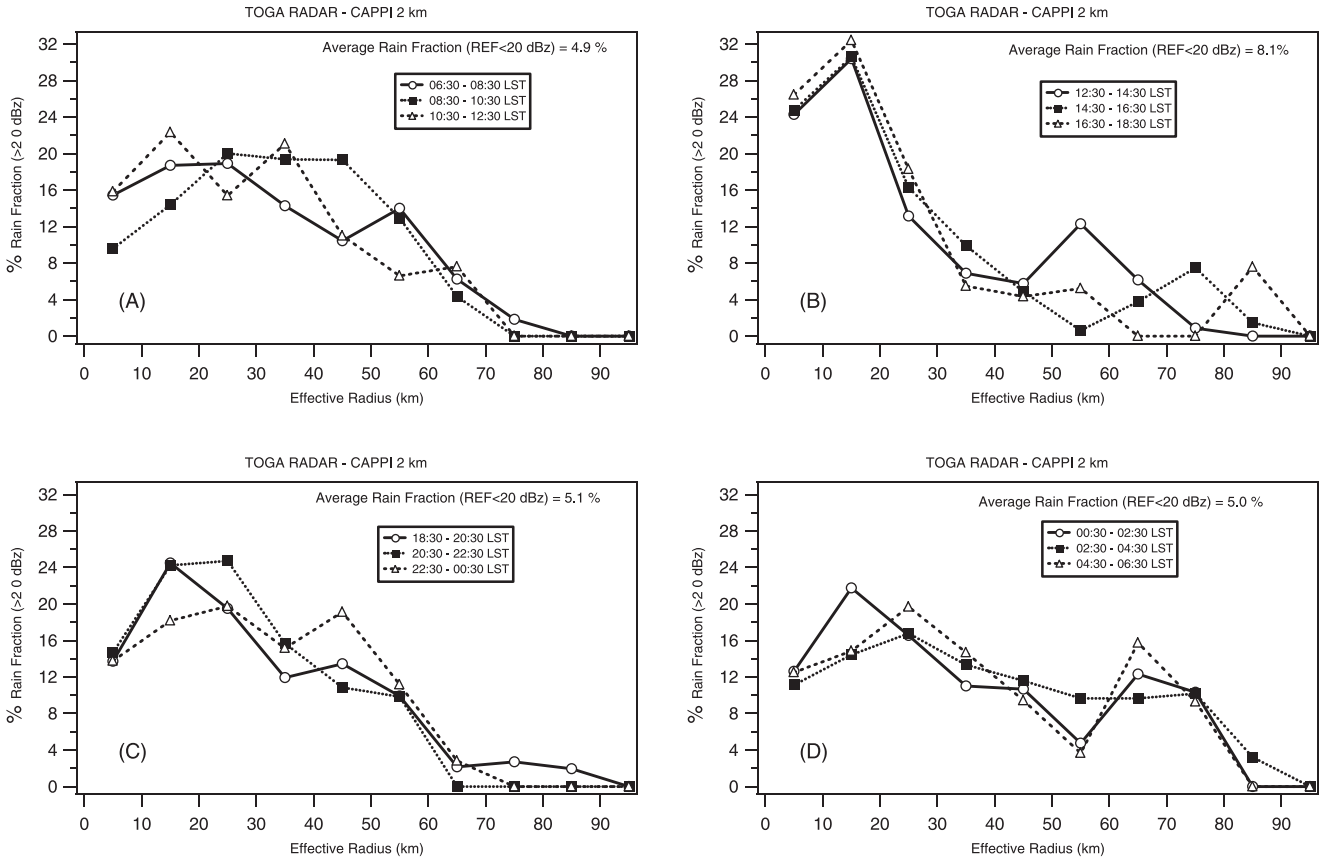

Figure 7. Rain cells size distribution as function of the diurnal cycle. Rain cells were defined using the threshold of 20 dBZ. Distributions are presented as the two-hours average. The curves show the contribution to the total rain fraction at specific time by different rain cells radius size.

around 70 km radius is very clear. It is related to the size organization of the nocturnal rain cells associated with low reflectivities values discussed in the previous section.

[34] In the afternoon, time of maximum convection, the size distribution has a different behavior from the other times of the day. There is a well-defined maximum for 15 km followed by an important decrease up to 40 km radius. We can also note the size evolution of large rain cells system increasing from 55 km at 1230–1430 LST to 85 km at 1630–1830 LST. The time evolution is consistent by showing the size increase of the rain cells in the afternoon. However, the contribution to the total rain fraction for these structures, larger than 50 km, is very small and probably is not a systematic feature.

[35] The convective system (Tir < 235 K) and rain cell (REF > 20 dBZ) structures were followed in time using the methodology described by *Mathon and Laurent* [2001]. This methodology permits us to describe the life cycle of the convective system and the rain cells and to establish the time and location of the spontaneous initiations and dissipations. The initiations due to split and the dissipations due to merge of convective systems or rain cells, as well as, the initiations or the dissipations due to an interval of missing images, have not been considered here. The tracking method was applied on satellite and radar images, for the convective systems and rain cells crossing the LBA region, see *Laurent et al.* [2001] for more details.

[36] Figures 8a and 8b present the hourly average of the convective system and rain cell spontaneous initiations and dissipations and the average rainfall computed from the four rain gauge networks. The maximum rain fraction (Figure 2b) occurs around 1300–1400 LST. At this time the majority of the convective systems and rain cells have a small size (Figures 6 and 7) and have the maximum area fraction increasing rate (Figure 2a). Figure 8 shows that the maximum precipitation occurs at this time.

[37] Initiations of convective systems and rain cells take place around the same time (1330 LST) of maximum precipitation. Maximum rain cell dissipation occurs one hour later at the time when the average precipitation rapidly decreases. Convective systems have longer and more variable lifetime durations. Convective system dissipation occurs 3 to 11 hours after the initiation, nevertheless, maximum dissipation occurs 5 hours after initiation. Rain cells present a secondary maximum of initiation, at 1830 LST, in agreement with a secondary maximum in precipitation. This secondary maximum in the initiation is associated with a peak of dissipation two-hour later. The nocturnal squall lines that crossed the LBA region are not present in the initiation and dissipation curves, probably because these convective systems are associated with a few long-lived convective systems that were generated earlier. As mentioned before, Figure 8 considers only the sponta-

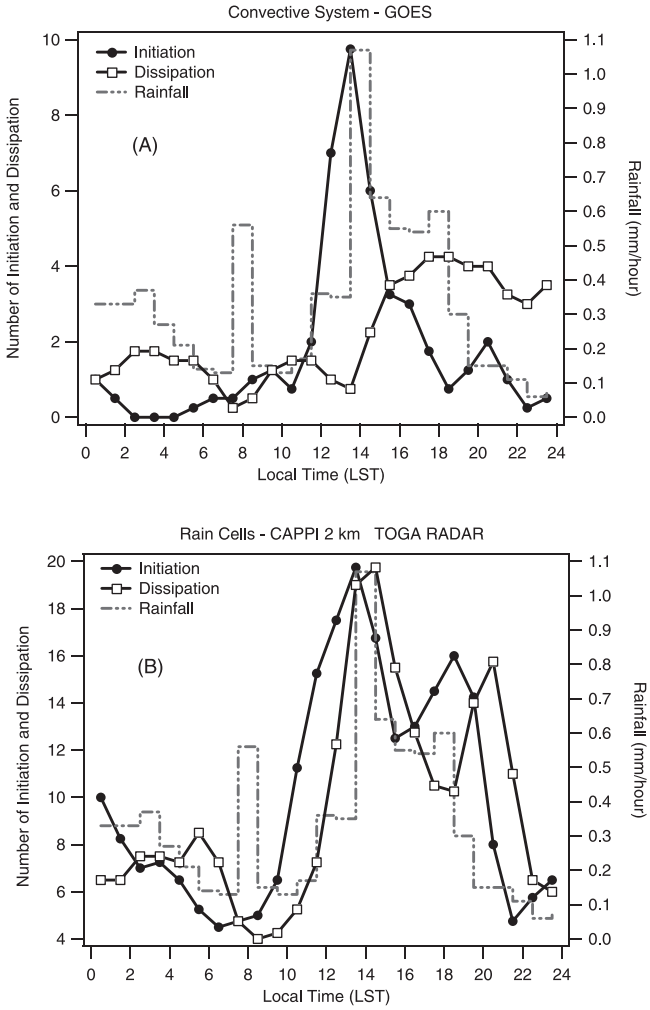

Figure 8. Hourly average precipitation for the 4 networks and the number of initiation and dissipation of the convective system (a) and rain cells (b).

neous initiation. The maximum merge occurred two hours after the maximum initiation at the time of the maximum high cloud fraction (figure not shown). It points to the fact that high cloud cover and convective system size increases are partially due to the merge of individual convective systems.

[38] As discussed before the variability is higher for the rain features than for the cloudiness. The time interval between initiation and dissipation is much larger for cloud systems than for rain cells. This result shows that the mesoscale cloudiness associated to the convective system has a longer life cycle than the rain feature within the convective system. *Machado et al.* [1998] showed that the size of convective systems increases somewhat more rapidly than it decreases. They also found that the size of the convective cells embedded inside the convective systems begin to decrease 3–6 hours before the whole convective system size begins to decrease.

5. Thermodynamic Structure

[39] Figure 9 shows an example of the time evolution of the ensemble of parameters described in the previous section over a 24 hours period. The sequence from 16 February 1200 LST to 17 February 1200 LST was chosen because it is well representative of the mean pattern. The minimum total cloud cover, for the day 16, occurs around 1300 LST; one hour later we observe an important increase in the convective rain and high cloud fraction, associated with a large amount of precipitation at about 1500 LST. Two hours later the high cloud cover reaches its maximum associated with weak precipitation. The total cloud cover presents a secondary maximum, 3 to 5 hours after the precipitation peak, followed by a decrease around 2300 LST. At this time the total cloud cover increases again and neither more rain fraction nor high cloud cover is observed. During the morning, cloud cover rapidly decreases to reach its minimum around 1200 LST.

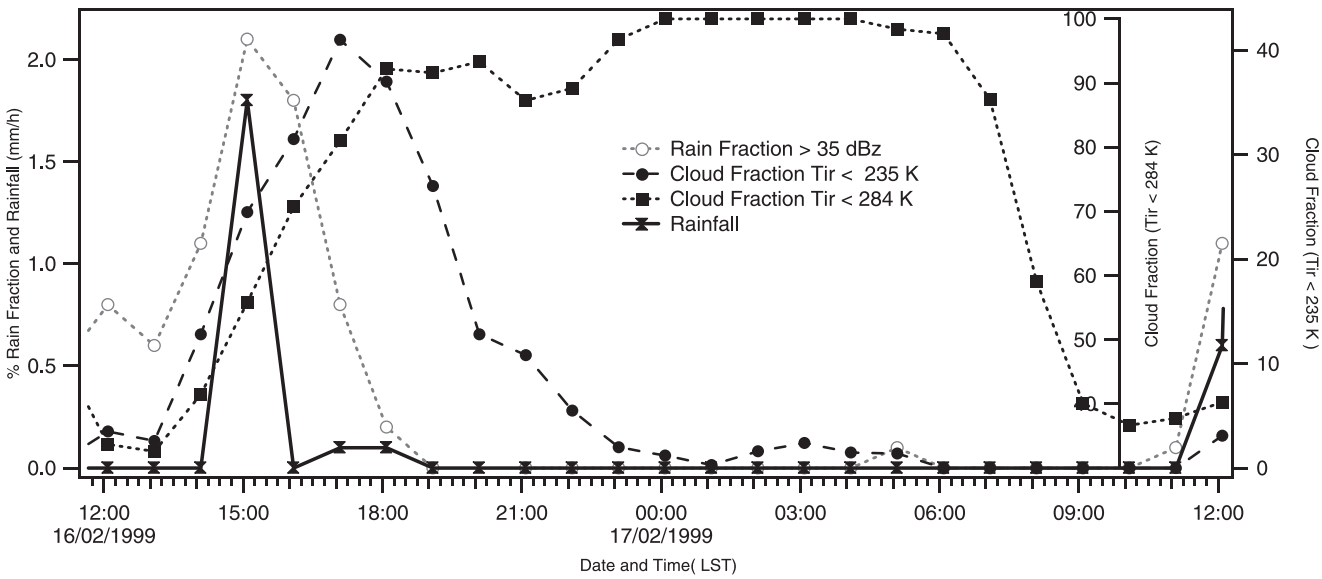

Figure 9. Evolution of the rain fraction (>35 dBZ), cloud fraction (<284 K), cold cloud fraction (<235 K), and rainfall (the average 4 networks) from 16 February at 1200 LST to 17 February at 1200 LST.

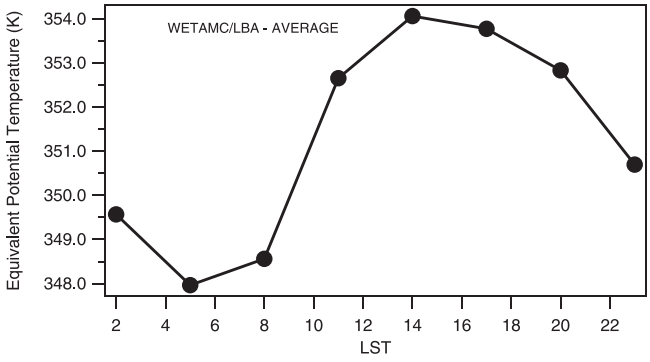

Figure 10. Hourly average for all radiosonde sites of the surface (the first 40 hPa layer) equivalent potential energy.

[40] As shown by radar and rain gauge data, precipitation occurs very rapidly in the early afternoon close to the time of minimum total cloud cover and at the time when high and convective clouds have the maximum area fraction increase rate and also when the initiation of convective systems and rain cells are the most numerous. The question that rises is why the maximum precipitation occurs just at the time of initiation when rain cells have a small size. It suggests that this explosive precipitation occurs because at this time the precipitating processes are very efficient; the large amount of water vapor advected in the convective towers is rapidly precipitated. Other studies [e.g., *McAnelly et al.*, 1997] have also observed the heaviest rainfall occurring near the time of convective initiation. At the early stage of convection, precipitation seems to be very efficient but later this efficiency decreases because part of the water vapor flux is advected to feed the stratiform anvil of the convective systems. *Gamache and Houze* [1983] studying GATE squall lines concluded that horizontal transfer of liquid water from convective towers into stratiform region of the cloud system created the majority of stratiform cloud.

[41] Another question that raise is why precipitation occurs in the early afternoon close to the time of minimum total cloud cover and why precipitation and high and convective cloud cover decreases in the end of the afternoon. The diurnal cycle of radiative forcing ultimately causes diurnal variations in the cloudiness. The large magnitude of the diurnal variation in insolation affects indirectly the surface radiation budget. The interaction of cloudiness and insolation depends on the thermodynamic characteristics of the atmosphere. To answer these questions this section discusses the thermodynamic characteristic observed during the experiment.

[42] The thermodynamic characteristics of the WETAMC/LBA are based on the analysis of the vertical profiles of temperature and humidity. Because surface measurements are very dependent on the local conditions and independent of the radiosonde measurements the first radiosonde level was computed as the average of the first 40 hPa layer (typical height of the mixed layer) to give an information not biased by surface observations and representative of the mean mixed layer conditions.

[43] Thermodynamic plays an important role in the energy exchanges in the atmosphere. The energy supplied for convection depends on the properties of the boundary layer and on the environment temperature. One of the most common parameters to analyze the energy available in the boundary layer to generate convection is the convective available potential energy (CAPE). The CAPE is useful to measure the amount of buoyancy in the atmosphere to drive updrafts. The CAPE was largely used to study deep convection [e.g., *Zipzer and LeMone*, 1980; *Jorgensen and LeMone*, 1989; *Mapes and Houze*, 1992; *Williams and Renno*, 1993].

[44] The present analysis was performed calculating the thermodynamic parameters for each site, based on work by *Bolton* [1980], *Emanuel* [1994], and *Wallace and Hobbs* [1977]. The CAPE was computed considering a pseudo-adiabatic process of an unmixed parcel ascending in the atmosphere (see equation (4)). Instability (N^2) was calculated as the Square of Brunt Vaisala frequency (see equation (5)). The thickness of the positive buoyancy layer [TPBL] was calculated as the difference between the LFC (Level of Free Convection), the first level when the parcel is warmer than the environment, and the LNB (Level of Neutral Buoyancy), the first level (after LFC) when the parcel is colder than the environment. The inhibition, the layer in which the parcel needs energy to move up because of the negative buoyancy, was computed as the difference between LCL (Lifting Condensation Level) and LFC.

$$CAPE = \int_{LFC}^{LNB} R_d\left(Tv_p - Tv_e\right) LnP \tag{4}$$

where, Tv_p and Tv_e are the virtual temperature of an air parcel lifted from the surface and the environment virtual temperature; R_d is the dry air gas constant and P is the pressure.

$$N^2 = \frac{g}{\theta_v}\frac{\partial \theta_v}{\partial z} \tag{5}$$

where, θ_v is the equivalent virtual temperature and δz corresponds to the difference between surface (the average of the first 40 hPa layer) and the level 40 hPa higher.

[45] The CAPE is very sensitive to small changes in the surface temperature, humidity, and pressure [*Mapes and Houze*, 1992]. However, the density profile of the upper troposphere, in the tropical regions, is more stable accounting for less significant variations and having a minor influence in the CAPE value [*Ye et al.*, 1998]. Large CAPE values are then mainly defined by surface parameters (θ_e); surface parameters are strongly affected by surface fluxes (local processes) and advection (small scale downdraft or large scale subsidence).

[46] The hourly average θ_e for all radiosonde stations is presented in Figure 10. We can see that in the morning there is an important increase in the θ_e mainly at the time of the minimum total cloud cover, which corresponds also to the time when maximum solar radiation reaches the surface. Around 1400 LST, θ_e reaches the maximum value around 354 K, decreasing after 1700 LST. During the night the mean θ_e weakly changes with time, maintaining a value around 349 K. The diurnal variation of θ_e, that rapidly increase with the solar insolation and reaches the maximum at the time of minimum total cloud cover is in good agreement with the convective activity and the time of the maximum precipitation.

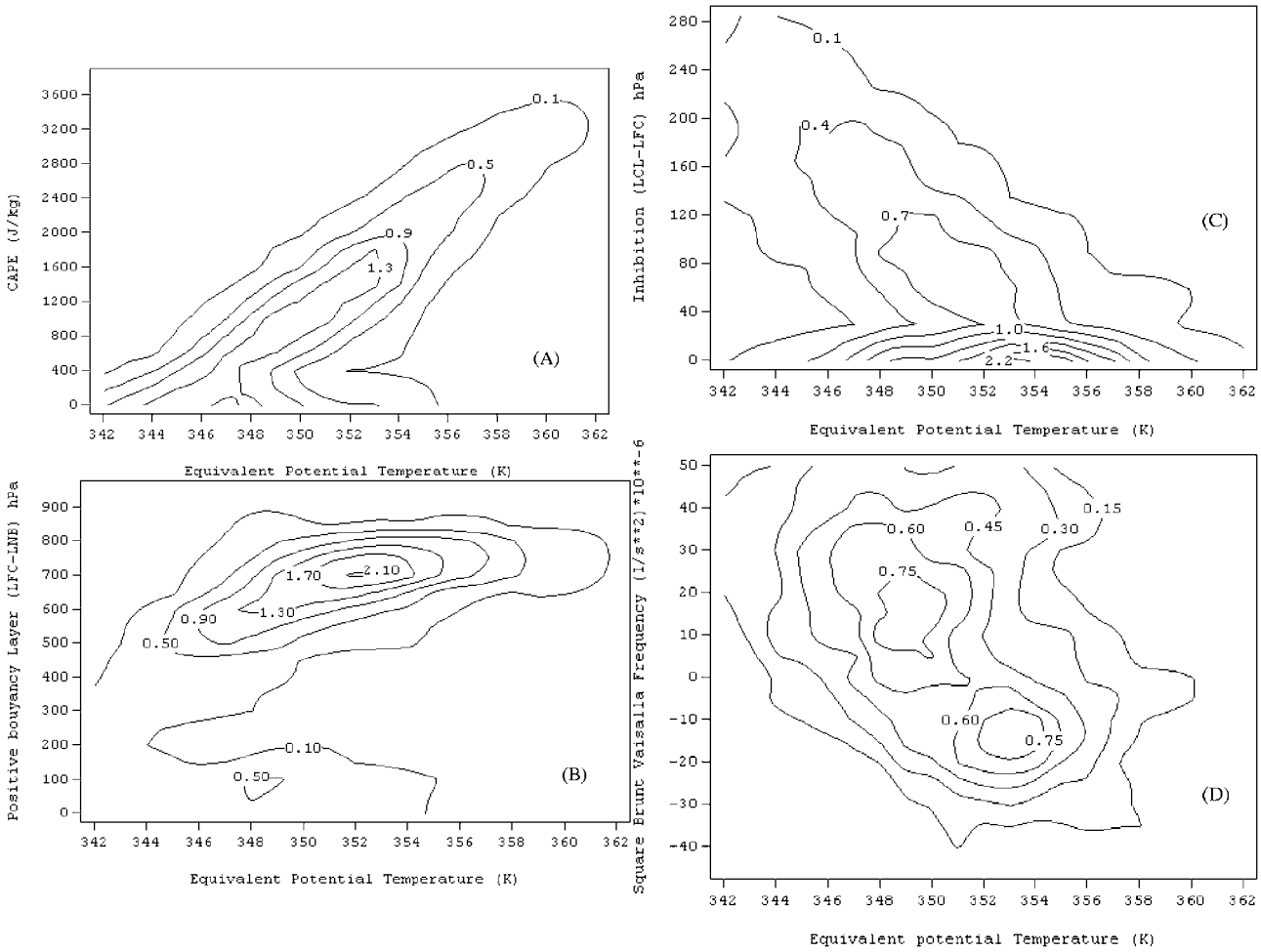

Figure 11. Relationship between surface (the first 40-hPa layer) equivalent potential energy, for all sites, and CAPE (a), the thickness of the layer between level of free convection and level of neutral buoyancy (b), the thickness of the layer between the lift condensation level and the level of free convection (c) and the Square of the Brunt Vaisalla Frequency (d). Values correspond to the probability of occurrence.

[47] Figure 11 shows the relationship between θ_e and CAPE (Figure 11a), TPBL (Figure 11b), Inhibition (Figure 11c) and the square of the Brunt Vaisala frequency (Figure 11d).

[48] A linear relationship between CAPE and surface θ_e or θw was proposed by *Mapes* [1993] and *Williams and Renno* [1993]. *Ye et al.* [1998] using GCM model showed that the almost perfect linear relationship between CAPE and wet-bulb potential temperature (θw) is primarily due to the surface evaporation. The analysis of our data is coherent with this quasi-linear relation between CAPE and θ_e. However, we note that for θ_e values smaller than about 356 K two features can be identified: One is a linear relation between CAPE and θ_e and the other is CAPE close to zero independently of θ_e. However, for larger θ_e values, larger than 356 K, a linear relation is well adapted and corresponds to the population of large CAPE. These large CAPE values mainly occur in the early afternoon in agreement with the hourly evolution of the θ_e as shown in Figure 10.

[49] Figure 11b shows θ_e as a function of the TPBL. As for Figure 11a, we can observe two different behaviors: For the TPBL between 150 and 800 hPa, the TPBL increases exponentially as a function of θ_e. For TPBL smaller than 150 hPa θ_e is not function of the TPBL. Small values of CAPE are more associated to the TPBL than the θ_e (not shown). It seems that CAPE is a function of θ_e when the atmosphere is far from its equilibrium state; otherwise the CAPE strongly depends on the atmosphere temperature and humidity profiles. The population of TPBL smaller than 150 hPa is the same as the CAPE uncorrelated with θ_e. It seems that the atmosphere first reaches the equilibrium state to decrease the surface θ_e later. These results suggest that the surface equivalent potential temperature increases due to the surface flux as a result of the large amount of solar energy reaching the surface in the morning and as a consequence TPBL and CAPE increase. The CAPE increases as θ_e increases by increasing the magnitude of the buoyancy in each pressure level. In the early afternoon when large CAPE (θ_e) values are found, convection develops changing the environment, modifying the structure of the atmosphere toward the reference of quasi equilibrium state. Parcels rising in the atmosphere have less and less buoyancy

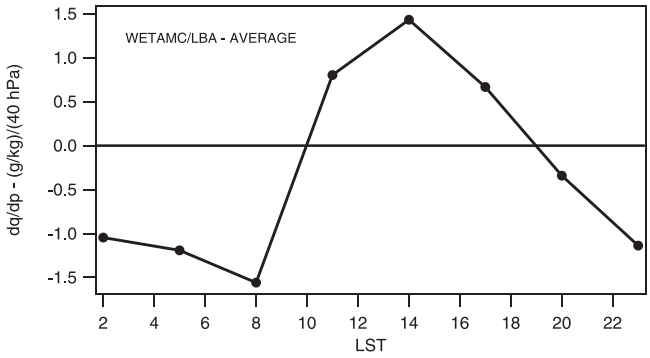

Figure 12. The diurnal cycle of the specific humidity gradient between the first 40-hPa layer and the subsequent layer 40 hPa higher, computed for all sites.

because the environment becomes nearly saturated, close to the equivalent potential temperature of saturation.

[50] The air close to the surface when rising adiabatically has negative buoyancy up to its LFC (except when the surface temperature reaches the convective temperature). This layer of negative buoyancy is essential to prevent spontaneous release of available potential energy and to accumulate potential buoyancy energy [*Emanuel et al.*, 1994]. If the existence of a negative buoyancy layer is substantial to the convection (mainly to the organization of the convection) it is an inhibition for the convective processes. The height of the LFC defines the degree of inhibition, i.e., the quantity of energy that needs to be supplied to the surface air parcels to reach the layer of positive buoyancy. Figure 11c shows the relationship between inhibition, computed as LCL-LFC, and θ_e. We can observe a nearly linear relation; large θ_e values, especially those close to the early afternoon θ_e value (>356 K) are associated with a thin layer of negative buoyancy.

[51] The relationship between θ_e and the instability, here presented as the square of the Brunt Vaisalla frequency (Figure 11d) also shows a nearly linear relationship with θ_e although with a larger dispersion; however, θ_e values larger than 356 K are mainly associated with an unstable boundary layer.

[52] Results from Figure 11 show how the insolation after the sunrise modulates the thermodynamics. We can notice a positive feedback: In the morning insolation increases and cloud cover decreases increasing the energy reaching the surface, up to the time of the beginning of the convection; the higher the θ_e the lower the inhibition, the higher the CAPE and the more unstable the atmosphere, favoring the development of the convection.

[53] The relationship between θ_e and high cloud fraction (not shown) demonstrate that the majority of high values of θ_e are associated with small high cloud fraction. When the cloud cover is high, θ_e (CAPE) has already been used to move the atmosphere to the equilibrium state. *Reed and Recker* [1971] studying Easterly Waves during GATE and *Mapes and Houze* [1992] studying mesoscale convective systems during the EMEX also found low values of CAPE associated with high cloud cover. This behavior explains the difference of about two hours between the θ_e maximum and the maximum of high cloud cover described in the previous section. The time needed by the convection to adjust to the reference profile is discussed by *Betts and Miller* [1986].

[54] The net vertical flux of water vapor across the boundary layer is proportional to the specific humidity gradient. The rate of transfer of water vapor in the boundary layer (evaporation) depends on many factors as, for example, the surface roughness and the vertical gradient of specific humidity. *Peixoto and Oort* [1992] estimated the evaporation (E) as a gradient flux by the relation:

$$E = -\rho\alpha_w \frac{\partial q}{\partial z} \tag{6}$$

where α_W is the molecular diffusivity for water vapor, ρ is the air density near surface, and q is the specific humidity of saturation in the boundary layer.

[55] Figure 12 shows the diurnal cycle of the specific humidity gradient (pressure coordinate). We can notice that the maximum water vapor flux in the boundary layer occurred in the early afternoon followed by a rapid decrease. After 1800 LST up to 1000 LST, in the next morning, we do not observe, in the average, water vapor flux from the surface to the atmosphere. When θ_e is higher the specific humidity gradient ($\delta q/\delta p$) is positive and a larger evaporation or a water vapor flux in the boundary layer is expected. For the conditions of low θ_e values $\delta q/\delta p$ is nearly zero or negative decreasing or extinguishing the water vapor flux to the atmosphere.

[56] For the majority of the cases, the convection is initiated by small-scale updrafts mainly during the time of minimum cloud cover, when values of θ_e are large (high CAPE, atmosphere unstable, deep layer of positive buoyancy and small layer of inhibition), initiating a large number of convective cells. When the cloud cover increases, the convection acts as a negative feedback damping the convection, saturating the boundary layer and extinguishing the water vapor flux. While the convective cloud cover is important the surface is nearly saturated and the lower atmosphere is strongly stable (not shown). The downdrafts stabilize the subcloud layer by cooling and drying the atmosphere. *Yano and Emanuel* [1991] improved the WISHE model [*Emanuel*, 1987] by explicitly taking into account this feature. After convection reached the maximum activity, the nearly saturated subcloud layer can be explained by three processes: (1) the evaporation of the precipitation in the subcloud layer, not taken into account in the WISHE model, is an important parameter in the moist entropy budget. (2) The effect of cooling by downdraft, decreasing the mixing ratio of saturation, is more important than the drying effect that decreases the sub cloud layer mixing ratio. (3) Surface flux of water vapor feeds the subcloud layer and this one feeds with water vapor the deep troposphere. When the specific humidity gradient in the lower atmosphere is nearly null, the boundary layer cannot export this water vapor and become saturated.

[57] Based on the discussion above, we propose the following hypothesis to describe the behavior of the local convection in the Amazon Basin: During the night the surface temperature decreases by radiative cooling building a low level inversion and decreasing the boundary layer height. However, the large amount of cloud cover observed at this time, limits the radiative cooling, which may explain the small differences between pasture and forest sites (Fisch

et al., submitted manuscript, 2001). The Amazon region receives more solar radiation than it loses by radiative cooling, and as the atmosphere is in statistical equilibrium, the atmosphere exports this excess of energy by convection. The high cloud cover during the night reduces the OLR (Outgoing Longwave Radiation) therefore the atmosphere needs more convection to export this excess of energy stored during the night. During the first hours of the day the heating of solar radiation breaks the low level inversion, and the boundary layer rapidly increases [*Fisch*, 1996]. Cloud cover decreases in the morning, which increases the solar flux reaching the surface, and consequently increases the equivalent potential energy. At this time, the boundary layer has the possibility to receive large amounts of water vapor by surface latent flux (it is essentially unsaturated and there is large gradient of specific humidity - Figure 12). If the surface reaches the convective temperature or if there is an orographic forcing (*Laurent et al.* [2001], show the importance of the orography in the convection generation during the TRMM-WETAMC/LBA) the air parcel can rise even without any large-scale forcing. Consequently the LFC decreases, the surface wind increases by boundary layer convergence which increase evaporation and convection rapidly develops. After the convection is developed, the atmosphere profile is modified to the nearly saturated state; the boundary layer becomes saturated and very stable, decreasing the surface flux and consequently extinguishing the convection.

6. Summary

[58] The TRMM-WETAMC/LBA experiment provides an opportunity to study the tropical convection in the Amazon Basin. The combination of different instrumentations such as radar, satellite images, rain gauge network, and radiosondes is a unique and robust database for fundamental studies of cloud and precipitation processes. This work studied the diurnal variation of the different types of clouds observed by satellite, intensities of rain cells observed by radar and precipitation and their relationships with thermodynamic parameters.

[59] High and convective cloud areas reach their maximum some hours after the maximum rainfall detected by rain gauge and radar 2 km CAPPI. The minimum cloud cover occurs only a few hours before the maximum of precipitation and the maximum cloud cover occurs during the night. The maximum rainfall takes place at the time of the maximum number of initiation of the convective systems observed by satellite and rain cells observed by radar. Rain cells have a typical lifetime of about one hour but for convective systems, dissipations take place from 3 to 11 hours after initiation with a dissipation maximum occurring about 5 hours later. At the time of maximum of precipitation (and rain fraction) the majority of the convective systems and rain cells are small sized and present the maximum increasing rate.

[60] The diurnal evolution of the equivalent potential temperature also presents a very clear diurnal variation with a maximum occurring in the early afternoon. The CAPE is well related to the θ_e; when θ_e is high (above 356 K) CAPE values are high, the atmosphere is unstable, a deep layer of positive buoyancy is developed and the inhibition layer is very shallow. About four-five hours after the precipitation maximum, high-level cloud fraction reaches its maximum, θ_e decreases, and the atmosphere boundary layer reduces the water vapor flux to the atmosphere.

[61] The general description above, suggests the following mechanism controlling the diurnal cycle of convection: In the morning, the cloud cover decreases as the insolation and solar flux reaching the surface increases and consequently θ_e also increases. The boundary layer has the ability to receive a large amount of water vapor by surface latent flux because there is a large specific humidity gradient. In the early afternoon the convection develops rapidly, the high and convective cloud fraction increase rapidly, and the maximum of precipitation and initiation is observed. The large amount of water vapor advected in the convective towers is rapidly precipitated. It is suggested that the latent heat released by the convective towers in the middle atmosphere will contribute to a later development of large cloud clusters. These hypotheses explain the later maximum in convective and high cloud fraction and the large number of convective systems merge and the precipitation reduction. The precipitation efficiency decreases probably because part of the water vapor flux is advected to the anvil creating the stratiform parts of the convective systems. Between the initiation and the dissipation of the convective systems the atmosphere profile is modified to reach a nearly saturated state; the boundary layer becomes saturated and very stable, which inhibits the surface fluxes and consequently extinguishes the convection.

[62] **Acknowledgments.** This study was supported by Conselho Nacional de Desenvolvimento Cientifico e Tecnólogico (CNPq), Brazil/Institut de Recherche pour le Développement, France (IRD) cooperative project grant 910153/98-1. The work has also received financial support from the Fundação de Amparo à Pesquisa do Estado de São Paulo (FAPESP) grant 99/06045-7 and FAPESP grant 1997/9926-9. The authors especially thank Carlos Morales and Dirceu Herdies for the radar and satellite data process and all the participants of the LBA campaign, especially Maria Assunção F. Silva Dias for her effort and dedication in managing the Brazilian components of the experiment. We would like to thank William Rossow and the anonymous reviewers for their comments and suggestions to the manuscript.

References

Betts, A. K., and M. J. Miller, A new convective adjustment scheme, part II, Single column tests using GATE wave, BOMEX, ATEX and arctic airmass data sets, *Q. J. R. Meteorol. Soc.*, *112*, 693–709, 1986.

Bolton, D., The computation of equivalent potential temperature, *Mon. Weather Rev.*, *108*, 1046–1053, 1980.

Chen, S. S., and R. A. Houze Jr., Diurnal variation and life-cycle of deep convective systems over the tropical Pacific warm pool, *Q. J. R. Meteorol. Soc.*, *123*, 357–388, 1997.

Cohen, J. C. P., M. A. F. Silva Dias, and C. A. Nobre, Environmental conditions associated with Amazonian squall lines: Case study, *Mon. Weather Rev.*, *123*, 3163–3174, 1995.

Cotton, W. R., and R. A. Anthes, *Storm and Cloud Dynamics*, 880 pp., Academic, San Diego, Calif., 1989.

Duvel, J. P., Convection over tropical Africa and the Atlantic Ocean during northern summer, part I, Interannual and diurnal variations, *Mon. Weather Rev.*, *117*, 2782–2799, 1989.

Duvel, J. P., and R. S. Kandel, Regional-scale diurnal variations of outgoing infrared observed by Meteosat, *J. Clim. Appl. Meteorol.*, *24*, 335–349, 1985.

Emanuel, K. A., An air-sea interaction model of intraseasonal oscillation in the tropics, *J. Atmos. Sci.*, *44*, 2324–2340, 1987.

Emanuel, K. A., *Atmospheric Convection*, 567 pp., Oxford Univ. Press, New York, 1994.

Emanuel, K. A., J. D. Neelin, and C. S. Bretherton, On large-scale circulations in convecting atmospheres, *Q. J. R. Meteorol. Soc.*, *120*, 1111–1143, 1994.

Fisch, G. F., *Amazon boundary layer: Observation and modeling aspects*, Ph.D. thesis (in Portuguese), Dep. of Atmos. Sci., Inst. Nac. de Pesquisas Esp., São José dos Campos, Brazil, 1996.

Gamache, J. F., and R. A. Houze Jr., Water budget of a mesoscale convective system in the Tropics, *J. Atmos. Sci.*, *40*, 1835–1850, 1983.

Garreaud, R. D., and J. M. Wallace, The diurnal march of convective cloudiness over the Americas, *Mon. Weather Rev.*, *125*, 3157–3171, 1997.

Garstang, M., H. L. Massie Jr., J. Halverson, S. Grego, and J. Scala, Amazon coastal squall lines, part I, Structure and kinematics, *Mon. Weather Rev.*, *122*, 608–622, 1994.

Guedes, R. L., and L. A. T. Machado, Characteristics of the cloud cover over the South America based in satellite images (in Portuguese), *Rev. Bras. Meteorol.*, *12*, 1–19, 1997.

Hendon, H. H., and K. Woodberry, The diurnal cycle of tropical convection, *J. Geophys. Res.*, *98*, 16,623–16,637, 1993.

Janowiak, J. E., P. A. Arkin, and M. Morrissey, An examination of the diurnal cycle in oceanic tropical rainfall using satellite and in situ data, *Mon. Weather Rev.*, *122*, 2296–2311, 1994.

Jorgensen, D. P., and M. A. LeMone, Vertical velocity characteristics of oceanic convection, *J. Atmos. Sci.*, *46*, 621–640, 1989.

Laurent, H., L. A. T. Machado, C. Morales, and L. Durieux, Characteristics of the amazonian mesoscale convective systems observed from satelite and radar during the WETAMC/LBA experiment., submitted to *J. Geophy. Res.*, *107*, 10.1029/2001JD000337, in press, 2002.

Machado, L. A. T., The Amazon energy budget using the ABLE-2B and FluAmazon data, *J. Atmos. Sci.*, *57*, 3131–3143, 2000.

Machado, L. A. T., and W. B. Rossow, Structural characteristics and radiative properties of tropical cloud clusters, *Mon. Weather Rev.*, *121*, 3234–3260, 1993.

Machado, L. A. T., M. Desbois, and J. P. Duvel, Structural characteristics of deep convective systems over tropical Africa and Atlantic Ocean, *Mon. Weather Rev.*, *120*, 392–406, 1992.

Machado, L. A. T., J. P. Duvel, and M. Desbois, Diurnal variations and modulation by easterly waves of the size distribution of convective cloud clusters over west Africa Ocean, *Mon. Weather Rev.*, *121*, 37–49, 1993.

Machado, L. A. T., W. B. Rossow, R. L. Guedes, and A. Walker, Life cycle variations of convective systems over the Americas, *Mon. Weather Rev.*, *126*, 1630–1654, 1998.

Maddox, R. A., Mesoscale convective complexes, *Bull. Am. Meteorol. Soc.*, *61*, 1374–1387, 1980.

Mapes, B. E., Gregarious tropical convection, *J. Atmos. Sci.*, *50*, 2026–2037, 1993.

Mapes, B. E., and R. A. Houze Jr., An integrated view of 1987 Australian monsoon and its mesoscale convective systems, part I, Horizontal structure, *Q. J. R. Meteorol. Soc.*, *118*, 927–963, 1992.

Mathon, V., and H. Laurent, Life cycle of the Sahelian mesoscale convective cloud systems, *Q. J. R. Meteorol. Soc.*, *127*, 377–406, 2001.

McAnelly, R. L., J. E. Nachamkin, W. Cotton, and M. E. Nicholls, Upscale evolution of MCSs: Doppler radar analysis and analytical investigation, *Mon. Weather Rev.*, *125*, 1083–1110, 1997.

Miller, D., and J. M. Fritsch, Mesoscale convective complexes in the Western Pacific region, *Mon. Weather Rev.*, *119*, 2978–2992, 1991.

Minnis, P., and E. F. Harrison, Diurnal variability of regional cloud and clear sky radiative parameters derived from GOES data, part II, November 1978. Cloud distributions, *J. Clim. Appl. Meteorol.*, *23*, 1032–1051, 1984.

Peixoto, J., and A. Oort, *Physics of Climate*, 520 pp., Am. Inst. of Phys., New York, 1992.

Reed, R. J., and E. E. Recker, Structure and properties of synoptic-scale wave disturbances in the equatorial western Pacific, *J. Atmos. Sci.*, *28*, 1117–1133, 1971.

Rickenbach, T. M., Cloud top evolution of tropical oceanic squall lines from radar reflectivity and infrared satellite data, *Mon. Weather Rev.*, *127*, 2951–2976, 1999.

Silva Dias, M. A. F., et al., Clouds and rain processes ina biosphere atmosphere interaction context in the Amazon region, submitted to *J. Geophys. Res.*, *107*, 10.1029/2001JD000355, in press, 2002.

Silva Dias, P. L., and J. P. Bonatti, A preliminary study of observed vertical mode structure of the summer over tropical South America, *Tellus, Ser. A*, *37*, 185–195, 1985.

Silva Dias, P. L., J. P. Bonatti, and V. E. Kousky, Diurnally forced tropical tropospheric circulation over South America, *Mon. Weather Rev.*, *115*, 1465–1478, 1987.

Wallace, J. M., and P. V. Hobbs, *Atmospheric Science. An Introductory Survey*, 465 pp., Academic, San Diego, Calif., 1977.

Williams, E., and N. Renno, An analysis of the conditional instability of the tropical atmosphere, *Mon. Weather Rev.*, *121*, 21–36, 1993.

Wu, X., and M. A. LeMone, Fine structure of cloud patterns within the intraseasonal oscillation during TOGA COARE, *Mon. Weather Rev.*, *127*, 2503–2513, 1999.

Yano, J. I., and K. Emanuel, Improved model of the equatorial troposphere and its coupling with stratosphere, *J. Atmos. Sci.*, *48*, 377–389, 1991.

Ye, B., A. D. Del Genio, and K. K. W. Lo, CAPE variations in the current climate and in a climate change, *J. Clim.*, *11*, 1997–2015, 1998.

Zipser, E. J., and M. A. LeMone, Cumulonimbus vertical velocity events in GATE, part II, Synthesis and model core structure, *J. Atmos. Sci.*, *37*, 2458–2469, 1980.

H. Laurent, A. A. Lima, and L. A. T. Machado, Divisão de Ciências Atmosféricas, Instituto de Aeronáutica e Espaço, Centro Técnico Aeroespacial, São José dos Campos, SP, Brazil.